

# A Speeding up Technique for Lossy Anisotropic Algorithm in FDTD Method

Fatih Kaburcu<sup>1</sup> and Atef Z. Elsherbeni<sup>2</sup>

<sup>1</sup>Electrical and Electronic Engineering Department  
Erzurum Technical University, Erzurum, 25700, Turkey  
fkaburcu@syr.edu, fatih.kaburcu@erzurum.edu.tr

<sup>2</sup>Electrical Engineering and Computer Science Department  
Colorado School of Mines, Golden, CO 80401, USA  
aelsherb@mines.edu

**Abstract**— In this paper, a speeding up technique for the lossy anisotropic (Lossy-ANI) algorithm integrated into the finite-difference time-domain (FDTD) method is proposed. The speeding up technique provides remarkable reduction in the computation time of the Lossy-ANI algorithm. This algorithm is applied to a line-fed microstrip patch antenna (MPA) with anisotropic substrate and a lossy anisotropic scattering object. Numerical results show that the anisotropy effects the resonant frequencies of the MPA and the bistatic RCS of the scattering object.

**Index Terms**— FDTD, lossy anisotropic medium.

## I. INTRODUCTION

A generalized 3D FDTD algorithm is formulated based on Lossy-ANI algorithm with a speeding up technique. The Lossy-ANI algorithm was first proposed in [1] for a one-dimensional Lossy-ANI scatterer with permittivity and electric conductor tensors. This algorithm was extended in [2-4] for the 3D Lossy-ANI scatterer with permittivity, permeability, magnetic, and electric conductor tensors. Algorithms for complex lossy mediums and lossy dielectric mediums with off-diagonal permittivity and conductivity tensors were proposed in [5] and [6], respectively. The 3D FDTD algorithm for the analysis of anisotropic materials faces a lot of challenges, such as requirement of large computer memory and long computation time. A speeding up technique, proposed in this paper to reduce the computation time is achieved by dividing the computation of fields into two parts in the FDTD simulation: one is the fields produced by off-diagonal elements of anisotropic tensors, and the other is the fields produced by diagonal elements of anisotropic tensors. Then, the sum of the fields are considered as the total fields for the next time-step in the simulation. This technique provides remarkable reduction in the

computation time.

A line-fed MPA with uniaxial anisotropic substrate was presented in [7]. Then, the MPA with anisotropic substrate was analyzed in [8-9] using the lossless anisotropic algorithm based on the relationships between  $D$ -,  $E$ -,  $B$ -, and  $H$ -fields. This example will be tested here but after the presentation of the new process of updating the FDTD equations.

In this paper, a detailed analysis of Lossy-ANI algorithm and speeding up technique are presented in Section II. The computational domain in the presented algorithm are terminated by the convolution perfectly matched layers (CPML). A line-fed MPA with anisotropic substrate and a lossy anisotropic scattering object are analyzed to investigate the simulation verification and its performance. Numerical results show that the scattering parameter of the MPA and the bistatic RCS of the scattering object are effected by the anisotropy as expected.

## II. LOSSY-ANI ALGORITHM

### A. Maxwell equations for 3D Lossy-ANI medium

The Maxwell equations for Lossy-ANI medium are:

$$\nabla \times H = \bar{\bar{\epsilon}} \frac{\partial E}{\partial t} + \bar{\bar{\sigma}}^e E \text{ and } \nabla \times E = -\bar{\bar{\mu}} \frac{\partial H}{\partial t} - \bar{\bar{\sigma}}^m H, \quad (1)$$

where  $\bar{\bar{\epsilon}}$ ,  $\bar{\bar{\mu}}$ ,  $\bar{\bar{\sigma}}^e$ , and  $\bar{\bar{\sigma}}^m$  are permittivity, permeability, electric and magnetic conductivity tensors, respectively. After some mathematical manipulation, one can obtain:

$$\begin{aligned} E^{n+1} &= \bar{\bar{p}}_e \cdot (\Delta \times H)^{n+\frac{1}{2}} + \bar{\bar{r}}_e \cdot E^n \\ H^{n+\frac{1}{2}} &= \bar{\bar{p}}_m \cdot (\Delta \times E)^n + \bar{\bar{r}}_m \cdot H^{n-\frac{1}{2}} \end{aligned} \quad (2)$$

where

$$\begin{aligned} \bar{\bar{p}}_e &= \left( \frac{\bar{\bar{\epsilon}}}{\Delta t} + \frac{\bar{\bar{\sigma}}^e}{2} \right)^{-1}, \bar{\bar{r}}_e = \bar{\bar{p}}_e \cdot \left( \frac{\bar{\bar{\epsilon}}}{\Delta t} - \frac{\bar{\bar{\sigma}}^e}{2} \right) \\ \bar{\bar{p}}_m &= \left( \frac{\bar{\bar{\mu}}}{\Delta t} + \frac{\bar{\bar{\sigma}}^m}{2} \right)^{-1}, \bar{\bar{r}}_m = \bar{\bar{p}}_m \cdot \left( \frac{\bar{\bar{\mu}}}{\Delta t} - \frac{\bar{\bar{\sigma}}^m}{2} \right) \end{aligned} \quad (3)$$

The  $x$ -component of the  $E$ - and  $H$ -fields in (2) are obtained after discretizing in space by the following equations:

$$E_x|_{i-\frac{1}{2},j,k}^{n+1} = \begin{pmatrix} p_{e11} \left( \frac{\partial H_z}{\partial y} \Big|_{i-\frac{1}{2},j,k}^{n+\frac{1}{2}} - \frac{\partial H_y}{\partial z} \Big|_{i-\frac{1}{2},j,k}^{n+\frac{1}{2}} \right) \\ + p_{e12} \left( \frac{\partial H_x}{\partial z} \Big|_{i-\frac{1}{2},j,k}^{n+\frac{1}{2}} - \frac{\partial H_z}{\partial x} \Big|_{i-\frac{1}{2},j,k}^{n+\frac{1}{2}} \right) \\ + p_{e13} \left( \frac{\partial H_y}{\partial x} \Big|_{i-\frac{1}{2},j,k}^{n+\frac{1}{2}} - \frac{\partial H_x}{\partial y} \Big|_{i-\frac{1}{2},j,k}^{n+\frac{1}{2}} \right) \\ + r_{e11} E_x|_{i-\frac{1}{2},j,k}^n + r_{e12} E_y|_{i-\frac{1}{2},j,k}^n + r_{e13} E_z|_{i-\frac{1}{2},j,k}^n \end{pmatrix}, \quad (4)$$

$$H_x|_{i,j,-0.5,k-0.5}^{n+0.5} = \begin{pmatrix} -p_{m11} \left( \frac{\partial E_z}{\partial y} \Big|_{i,j,-0.5,k-0.5}^{n+0.5} - \frac{\partial E_y}{\partial z} \Big|_{i,j,-0.5,k-0.5}^{n+0.5} \right) \\ -p_{m12} \left( \frac{\partial E_x}{\partial z} \Big|_{i,j,-0.5,k-0.5}^{n+0.5} - \frac{\partial E_z}{\partial x} \Big|_{i,j,-0.5,k-0.5}^{n+0.5} \right) \\ -p_{m13} \left( \frac{\partial E_y}{\partial x} \Big|_{i,j,-0.5,k-0.5}^{n+0.5} - \frac{\partial E_x}{\partial y} \Big|_{i,j,-0.5,k-0.5}^{n+0.5} \right) \\ -r_{m11} H_x|_{i,j,-0.5,k-0.5}^{n-0.5} - r_{m12} H_y|_{i,j,-0.5,k-0.5}^{n-0.5} \\ -r_{m13} H_z|_{i,j,-0.5,k-0.5}^{n-0.5} \end{pmatrix}, \quad (5)$$

where the first subscript of the coefficients ( $p_{e11}$ ,  $r_{e11}$ ,  $p_{m11}$ , and  $r_{e11}$ ) refers to the type of the field (electric or magnetic) and the second and third subscripts refer the element number of the matrix in (3).

Similarly, other components of  $E$ - and  $H$ -fields can be obtained. It is realized that  $i$ ,  $j$ , and  $k$  indices used in Equations (4)-(5) are not meant to give exact location where the fields are available. We must consider the exact location of the fields. Thus, linear interpolation [1-4] is used to obtain the right location of fields in the Yee's grid.  $E_y^n(i, j, k)$  and  $E_z^n(i, j, k)$  in (4) are interpolated from neighboring quantities as follows:

$$E_y^n(i, j, k) = \frac{1}{4} \begin{pmatrix} E_y^n(i+1, j+1, k) + E_y^n(i, j+1, k) \\ + E_y^n(i+1, j, k) + E_y^n(i, j, k) \end{pmatrix}, \quad (6.a)$$

$$E_z^n(i, j, k) = \frac{1}{4} \begin{pmatrix} E_z^n(i+1, j, k+1) + E_z^n(i, j, k+1) \\ + E_z^n(i+1, j, k) + E_z^n(i, j, k) \end{pmatrix}. \quad (6.b)$$

The spatial derivatives of  $H$ -fields in (4) can be obtained using the following approximations:

$$\frac{\partial H_z^{n+\frac{1}{2}}(i,j,k)}{\partial y} = \frac{1}{dy} (H_z^n(i, j+1, k) - H_z^n(i, j, k)), \quad (7.a)$$

$$\frac{\partial H_y^{n+\frac{1}{2}}(i,j,k)}{\partial z} = \frac{1}{dz} (H_y^n(i, j, k) - H_y^n(i, j, k-1)), \quad (7.b)$$

$$\frac{\partial H_x^{n+\frac{1}{2}}(i,j,k)}{\partial z} = \frac{0.25}{dz} \begin{pmatrix} H_x^n(i+1, j+1, k) + H_x^n(i, j+1, k) \\ + H_x^n(i+1, j, k) + H_x^n(i, j, k) \\ - H_x^n(i, j+1, k-1) - H_x^n(i+1, j, k-1) \\ - H_x^n(i+1, j+1, k-1) - H_x^n(i, j, k-1) \end{pmatrix}, \quad (7.c)$$

$$\frac{\partial H_x^{n+\frac{1}{2}}(i,j,k)}{\partial y} = \frac{0.25}{dy} \begin{pmatrix} H_x^n(i+1, j+1, k) + H_x^n(i, j+1, k) \\ + H_x^n(i+1, j, k-1) + H_x^n(i, j, k) \\ - H_x^n(i+1, j+1, k-1) - H_x^n(i, j+1, k-1) \\ - H_x^n(i+1, j, k-1) - H_x^n(i, j, k-1) \end{pmatrix}, \quad (7.d)$$

$$\frac{\partial H_z^{n+\frac{1}{2}}(i,j,k)}{\partial x} = \frac{0.25}{dx} \begin{pmatrix} H_x^n(i+2, j+1, k) + H_x^n(i+2, j, k) \\ - H_x^n(i, j+1, k) - H_x^n(i, j, k) \end{pmatrix}, \quad (7.e)$$

$$\frac{\partial H_y^{n+\frac{1}{2}}(i,j,k)}{\partial x} = \frac{0.25}{dx} \begin{pmatrix} H_y^n(i+2, j, k) + H_y^n(i+2, j, k-1) \\ - H_y^n(i, j, k) - H_y^n(i, j, k-1) \end{pmatrix}. \quad (7.f)$$

Now the  $x$ -component of the  $E$ -field in (4) can be updated using (6) and (7). Similarly, other component of the  $E$ - and  $H$ -fields can be updated. The spatial derivatives in the Yee's grids used in this paper have more complicated implementations compared to the Lebedev grids in [10].

## B. Speeding up technique

With this Lossy-ANI algorithm, the  $E$ - and  $H$ -fields are produced by off-diagonal elements of anisotropic tensors are calculated in the entire computational domain as in [1-4]. It is realized that a considerable amount of computation time is spent for the calculation of these fields. Therefore, a speeding up technique is proposed here to reduce the computation time. In this technique, the fields produced by off-diagonal elements of anisotropic tensors are calculated in the region-ANI shown in Fig. 1 that contains anisotropic object, whereas the fields produced by diagonal elements of anisotropic tensors are calculated in the entire computational domain. Then, the sum of these fields are considered as the total fields for the next time-step in the simulation. This technique provides more than 70% reduction in the computation time of the Lossy-ANI algorithm.

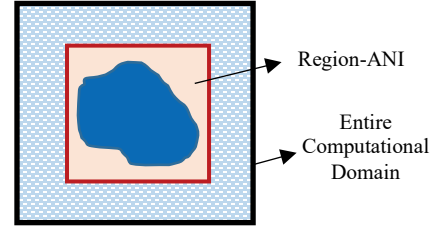


Fig. 1. Configuration of the FDTD computational domain for the Lossy-ANI algorithm.

## III. NUMERICAL RESULT

In this section, we test the performance of the Lossy-ANI algorithm with the speeding up technique for solving a line-fed MPA [11] with anisotropic substrate and an anisotropic scattering object. The computer being used in this work has Intel® Core™ i7-4790 CPU and 8 GB DDR RAM. The program is based on [12] and is written and compiled in 64-bit MATLAB version 8.2.0.701 (R2013b).

### A. A line-fed MPA with anisotropic substrate

A line-fed MPA with anisotropic substrate shown in Fig. 2 is analyzed to verify the efficiency of the Lossy-ANI algorithm with the speeding up technique. The discretization of the antenna in each direction are set to

$dx=0.3891$  mm,  $dy=0.4$  mm, and  $dz=0.1985$  mm. The rectangular patch size is  $(31 dx) \times (40 dy)$ . The size of the feed line is  $(6 dx) \times (30 dy)$ . The source and port position are located at the edge of the antenna. A Gaussian pulse is chosen as a source for the antenna. The simulation is performed for 6000 time steps.

The line-fed MPA with isotropic ( $\epsilon_r=2.2$  and  $\mu_r=1$ ) substrate is analyzed to prove the validity of the Lossy-ANI algorithm in comparison with that generated using the regular FDTD method. The scattering parameter ( $S_{11}$ ) of the MPA, shown in Fig. 3, shows good agreement. The operating resonant lowest and highest frequencies are 7.68 GHz and 18.04 GHz, respectively.

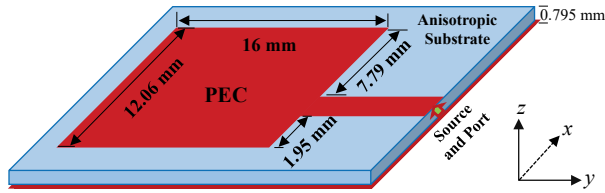


Fig. 2. A line-fed MPA with anisotropic substrate.

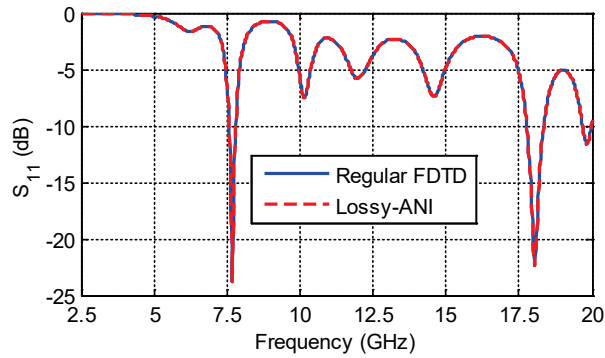


Fig. 3.  $S_{11}$  of the MPA with isotropic substrate obtained using the Lossy-ANI and the regular FDTD method.

Two different cases for the anisotropic substrate are then considered in new simulations. In the first case, the elements of permittivity and permeability tensors for the anisotropic substrate are given as follows:

$$\begin{aligned} \epsilon_{xx} &= \epsilon_1 \cos^2 \theta + \epsilon_2 \sin^2 \theta, \epsilon_{yy} = \epsilon_1, \epsilon_{zz} = \epsilon_1 \sin^2 \theta + \epsilon_2 \cos^2 \theta \\ \epsilon_{xz} &= \epsilon_{zx} = (\epsilon_1 - \epsilon_2) \sin \theta \cos \theta, \epsilon_{xy} = \epsilon_{yx} = \epsilon_{yz} = \epsilon_{zy} = 0 \\ \mu_{xx} &= \mu_1 \cos^2 \theta + \mu_2 \sin^2 \theta, \mu_{yy} = \mu_1, \mu_{zz} = \mu_1 \sin^2 \theta + \mu_2 \cos^2 \theta \\ \mu_{xz} &= \mu_{zx} = (\mu_1 - \mu_2) \sin \theta \cos \theta, \mu_{xy} = \mu_{yx} = \mu_{yz} = \mu_{zy} = 0 \end{aligned} \quad (8)$$

where  $\theta$  is the angle between the optical axis and the  $x$ -direction. For the second case, the elements of permittivity and permeability tensors for the anisotropic

substrate are then given as follows:

$$\begin{aligned} \epsilon_{xx} &= \epsilon_1, \epsilon_{yy} = \epsilon_1 \cos^2 \phi + \epsilon_2 \sin^2 \phi, \epsilon_{zz} = \epsilon_1 \sin^2 \phi + \epsilon_2 \cos^2 \phi \\ \epsilon_{yz} &= \epsilon_{zy} = (\epsilon_1 - \epsilon_2) \sin \phi \cos \phi, \epsilon_{xy} = \epsilon_{yx} = \epsilon_{xz} = \epsilon_{zx} = 0 \\ \mu_{xx} &= \mu_1, \mu_{yy} = \mu_1 \cos^2 \phi + \mu_2 \sin^2 \phi, \mu_{zz} = \mu_1 \sin^2 \phi + \mu_2 \cos^2 \phi \\ \mu_{yz} &= \mu_{zy} = (\mu_1 - \mu_2) \sin \phi \cos \phi, \mu_{xy} = \mu_{yx} = \mu_{xz} = \mu_{zx} = 0 \end{aligned} \quad (9)$$

where  $\phi$  is the angle between the optical axis and the  $y$ -direction. The material parameters in (8) and (9) are set to  $\epsilon_1=2.35$ ,  $\epsilon_2=2.05$ ,  $\mu_1=1.15$ , and  $\mu_2=0.85$ .

In the first case for the anisotropic substrate, the  $S_{11}$  as a function of  $\theta$  obtained using the Lossy-ANI algorithm is shown in Fig. 4. From Fig. 4, it can be observed that the lowest operating resonant frequency of the MPA is increasing if the angle  $\theta$  is decreasing from  $\pi/2$  to zero, whereas the highest operating resonant frequency of the MPA is decreasing. If the angle  $\theta$  is chosen to be zero,  $\pi/4$ , and  $\pi/2$ , the operating resonant frequencies of the MPA at the lowest operating resonant are 7.4, 7.22, and 6.88 GHz, respectively, whereas at the highest operating resonant, they are 17.44, 18.25, and 18.9 GHz, respectively. The ratio of the number of cells in the region-ANI to that in the entire computational domain is 6.46%.

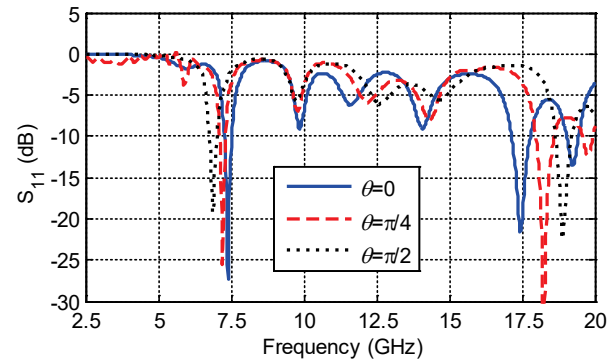


Fig. 4.  $S_{11}$  of the MPA as a function of  $\theta$  obtained using the Lossy-ANI algorithm.

In the second case for the anisotropic substrate with the same material parameters used in (9), the  $S_{11}$  as a function of  $\phi$  obtained using the Lossy-ANI algorithm is shown in Fig. 5. It can be observed from Fig. 5 that the operating resonance frequencies of the MPA are effected by the anisotropy in the substrate as those in the first case. The computation time of the MPA with the speeding up technique is 13 min 55 s, whereas those without the speeding up technique is 49 min 57 s. Therefore, the speeding up technique provides 72% reduction in the computation time.

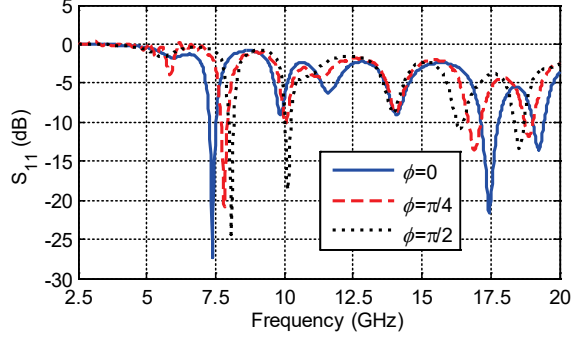


Fig. 5.  $S_{11}$  of the MPA as a function of  $\phi$  obtained using the Lossy-ANI algorithm.

### B. Lossy-ANI scattering object

To further verify the efficiency of the Lossy-ANI algorithm with the speeding up technique, a lossy anisotropic sphere with radius of 0.4 m, shown in Fig. 6, is analyzed. The discretization of the sphere in each direction is 0.025 m. This sphere is excited by a  $\theta$ -polarized plane wave with  $\theta^{\text{inc}}=90^\circ$  and  $\phi^{\text{inc}}=90^\circ$ . The simulation is performed for 2000 time steps.

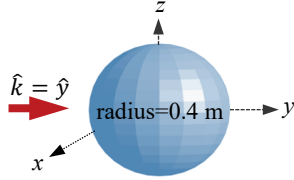


Fig. 6. Geometry of the lossy anisotropic sphere.

Three different cases for the anisotropic sphere are considered in this simulation. In the first case, the material parameters of the anisotropic sphere are given as follows:

$$\bar{\epsilon} = \epsilon_o \begin{bmatrix} 2.2 & 1.8 & 0 \\ 1.8 & 2.2 & 0 \\ 0 & 0 & 2.2 \end{bmatrix}, \bar{\mu} = \mu_o \begin{bmatrix} 2 & 1.6 & 0 \\ 1.6 & 2 & 0 \\ 0 & 0 & 2 \end{bmatrix}, \quad (10.a)$$

$$\bar{\sigma}^e = \begin{bmatrix} 0.85 & 0.7 & 0 \\ 0.7 & 0.85 & 0 \\ 0 & 0 & 0.85 \end{bmatrix} \frac{s}{m}, \bar{\sigma}^m = \begin{bmatrix} 0.65 & 0.5 & 0 \\ 0.5 & 0.65 & 0 \\ 0 & 0 & 0.65 \end{bmatrix} \frac{\Omega}{m}, \quad (10.b)$$

where  $\bar{\epsilon}$ ,  $\bar{\mu}$ ,  $\bar{\sigma}^e$ , and  $\bar{\sigma}^m$  are permittivity, permeability, electric and magnetic conductivity tensors, respectively. In the second case, the material parameters of the anisotropic sphere are given as follows:

$$\bar{\epsilon} = \epsilon_o \begin{bmatrix} 2.2 & 0 & 1.8 \\ 0 & 2.2 & 0 \\ 1.8 & 0 & 2.2 \end{bmatrix}, \bar{\mu} = \mu_o \begin{bmatrix} 2 & 0 & 1.6 \\ 0 & 2 & 0 \\ 1.6 & 0 & 2 \end{bmatrix}, \quad (11.a)$$

$$\bar{\sigma}^e = \begin{bmatrix} 0.85 & 0 & 0.7 \\ 0 & 0.85 & 0 \\ 0.7 & 0 & 0.85 \end{bmatrix} \frac{s}{m}, \bar{\sigma}^m = \begin{bmatrix} 0.65 & 0 & 0.5 \\ 0 & 0.65 & 0 \\ 0.5 & 0 & 0.65 \end{bmatrix} \frac{\Omega}{m}, \quad (11.b)$$

In the third case, the material parameters of the anisotropic sphere are given as follows:

$$\bar{\epsilon} = \epsilon_o \begin{bmatrix} 2.2 & 0 & 0 \\ 0 & 2.2 & 1.8 \\ 0 & 1.8 & 2.2 \end{bmatrix}, \bar{\mu} = \mu_o \begin{bmatrix} 2 & 0 & 0 \\ 0 & 2 & 1.6 \\ 0 & 1.6 & 2 \end{bmatrix}, \quad (12.a)$$

$$\bar{\sigma}^e = \begin{bmatrix} 0.85 & 0 & 0 \\ 0 & 0.85 & 0.7 \\ 0 & 0.7 & 0.85 \end{bmatrix} \frac{s}{m}, \bar{\sigma}^m = \begin{bmatrix} 0.65 & 0 & 0 \\ 0 & 0.65 & 0.5 \\ 0 & 0.5 & 0.65 \end{bmatrix} \frac{\Omega}{m}, \quad (12.b)$$

The bistatic RCSs for the three plane cuts ( $xy$ ,  $xz$ , and  $yz$ ) in Fig. 7 are computed at 300 MHz using the scattering fields from the anisotropic sphere for the three cases with the material parameters in (10)-(12) and compared with that generated using the scattering fields from the isotropic sphere when the material parameters are set to  $\epsilon_r=2.2$ ,  $\mu_r=2$ ,  $\sigma^e=0.85$ , and  $\sigma^m=0.65$ . It can be seen from Fig. 7 that the anisotropy in the sphere effects the magnitude of the RCS. The computation time of the anisotropic sphere with the speeding up technique is 4 min 12 s, whereas those without the speeding up technique 14 min 56 s. Therefore, the speeding up technique provides 72% reduction in the computation time for this scattering problem. The ratio of the number of cells in the region-ANI to that in the entire computational domain is 12.5%.

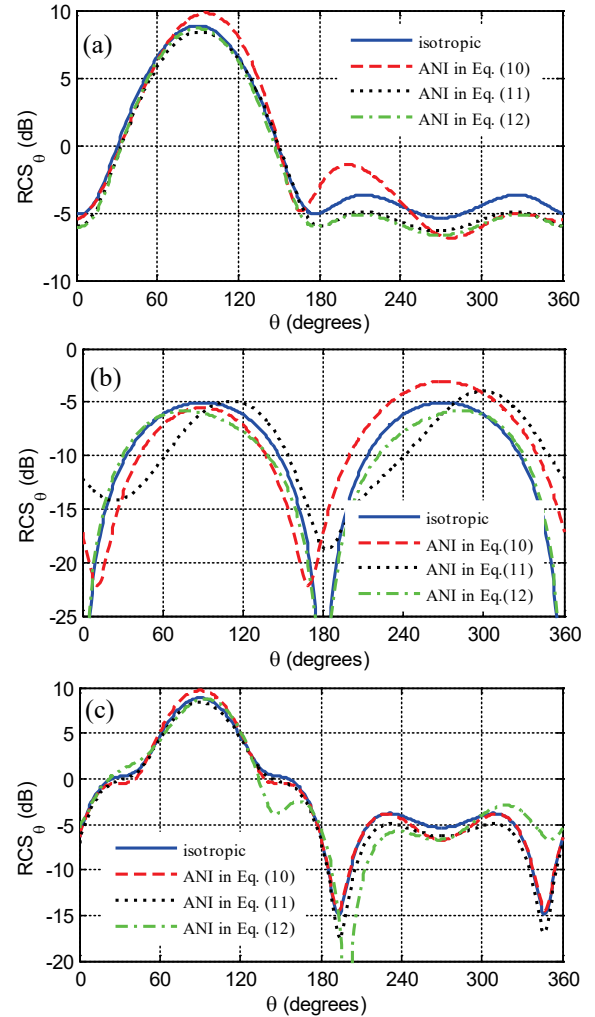


Fig. 7. Bistatic RCSs for: (a)  $xy$ , (b)  $xz$ , and (c)  $yz$  plane cuts.

#### IV. CONCLUSION

In this paper, the performance of a 3D FDTD algorithm based on the Lossy-ANI algorithm is presented in terms of computation time for solving the line-fed MPA with anisotropic substrate and the lossy anisotropic scattering object. The speeding up technique proposed here provides remarkable reduction in the computation time for configurations containing lossy anisotropic material. Numerical results show that the operating resonant frequencies of the MPA and magnitude of the bistatic RCS obtained from the scattering object are effected by the anisotropy of the material used.

#### REFERENCES

- [1] J. Schneider and S. Hudson, "The finite-difference time-domain method applied to anisotropic material," *IEEE Trans. on Antennas and Propagation*, vol. 41, pp. 994-999, July 1993.
- [2] D. Ge, L. Yang, B. Wei, N. Ge, and K. Zheng, "FDTD applied to lossy anisotropic medium and its parallel computing," *Proceedings of ISAP2005*, Seoul, Korea.
- [3] L. X. Yang, G. Wang, and S. Yan, "Parallel ANI-FDTD implementation for electromagnetic scattering by both electric and magnetic anisotropic medium," *Microwave and Optical Technology Letters*, vol. 50, no. 5, May 2008.
- [4] H. Zhang, Z. Li, Y. Wang, and J. Wang, "Studying on the parallel FDTD algorithm for calculating the EM scattering from anisotropic ellipsoid," *Cross Strait Quad-Regional Radio Science and Wireless Technology Conference (CSQRWC) IEEE, 2011*, vol. 1, 2011.
- [5] D. Vidacic, "Assesment of FDTD Model Parameters for Lossy Media," *Diss. University of New Hampshire*, 2003.
- [6] K.-Y. Jung, F. L. Teixeira, and R. Lee, "Complex envelope PML-ADI-FDTD method for lossy anisotropic dielectrics," *IEEE Antennas. Wireless Propag. Lett.*, vol. 6, pp. 643-46, 2007.
- [7] S. D. Gedney, "An anisotropic perfectly matched layer-absorbing medium for the truncation of FDTD lattices," *IEEE Trans. Antennas Propag.*, vol. 44, no. 12, pp. 1630-1639, Dec. 1996.
- [8] A. P. Zhao, J. Juntunen, and A. V. Raisanen, "An efficient FDTD algorithm for the analysis of microstrip patch antennas printed on a general anisotropic substrate," *IEEE Trans. Microwave Theory Tech.*, vol. 47, pp. 1142-1146, 1999.
- [9] L. Dou and A. R. Sebak, "3D FDTD method for arbitrary anisotropic materials," *Microw. Opt. Technol. Lett.*, vol. 48, no. 10, pp. 2083-2090, 2006.
- [10] M. Nauta, M. Okoniewski, and M. Potter, "FDTD method on a Lebedev grid for anisotropic

materials," in *IEEE Trans. Antennas Propag.*, vol. 61, no. 6, pp. 3161-3171, June 2013.

- [11] D. M. Sheen, S. M. Ali, M. D. Abouzahra, and J. A. Kong, "Application of the three-dimensional finite-difference time-domain method to the analysis of planar microstrip circuits," *IEEE Trans. Microwave Theory Tech.*, vol. 38, pp. 849-857, July 1990.
- [12] A. Z. Elsherbeni and V. Demir, *The Finite-Difference Time-Domain Method for Electromagnetics with MATLAB Simulations*. Second edition, ACES Series on Computational Electromagnetics and Engineering, SciTech Publishing, an Imprint of IET, Edison, NJ, 2016.



**Fatih Kaburcuk** was born in 1984, in Sivas, Turkey. He received both the M.Sc. and Ph.D. degrees from Syracuse University, Syracuse, New York in 2011 and 2014, respectively, all in Electrical Engineering. He worked as a Research Assistant for PPC-Belden, Inc., Syracuse, New

York in 2013. He worked as a Visiting Research Scholar in the Electrical Engineering and Computer Science Department at the Colorado School of Mines in 2014. Currently, Kaburcuk is working as an Assistant Professor at the Department of Electrical and Electronics Engineering at Erzurum Technical University, Erzurum, Turkey. His research interest includes electromagnetic scattering and microwaves.



**Atef Z. Elsherbeni** received his Ph.D. degree in Electrical Engineering from Manitoba University, Winnipeg, Manitoba, Canada, in 1987. He was with the University of Mississippi from 1987 to 2013 and was a Finland Distinguished Professor from 2009 to 2011. In August 2013

he became the Dobelman Distinguished Chair Professor of Electrical Engineering at Colorado School of Mines. His research interest includes the scattering and diffraction of EM waves, finite-difference time-domain analysis of antennas and microwave devices, field visualization and educational software development, interactions of EM waves with human body, RFID and sensor integrated FRID systems, printed antennas and antenna arrays, and measurement of material properties. Elsherbeni is a Fellow Member of IEEE and ACES. He is the Editor-in-Chief for ACES Journal. He was the General Chair for the 2014 APS-URSI Symposium and was the President of ACES Society from 2013 to 2015.